Nanoscale

Accepted Manuscript

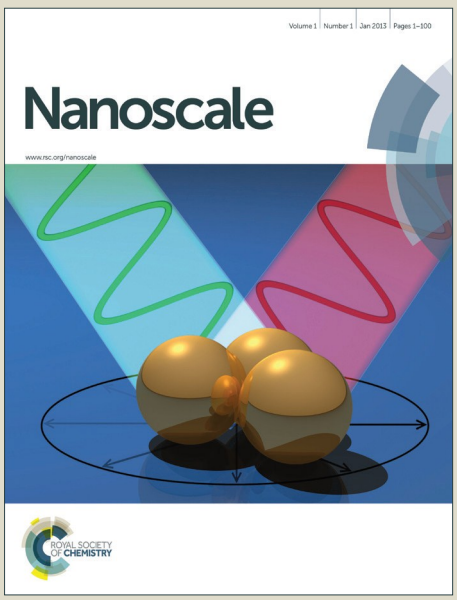

This is an *Accepted Manuscript*, which has been through the Royal Society of Chemistry peer review process and has been accepted for publication.

Accepted Manuscripts are published online shortly after acceptance, before technical editing, formatting and proof reading. Using this free service, authors can make their results available to the community, in citable form, before we publish the edited article. We will replace this *Accepted Manuscript* with the edited and formatted *Advance Article* as soon as it is available.

You can find more information about *Accepted Manuscripts* in the Information for Authors.

Please note that technical editing may introduce minor changes to the text and/or graphics, which may alter content. The journal's standard Terms & Conditions and the Ethical guidelines still apply. In no event shall the Royal Society of Chemistry be held responsible for any errors or omissions in this *Accepted Manuscript* or any consequences arising from the use of any information it contains.

ROYAL SOCIETY OF CHEMISTRY

www.rsc.org/nanoscale

Please do not adjust margins

Nanoscale

ARTICLE

Perovskite-organic hybrid tandem solar cells using nanostructured perovskite layer as light window and PFN/doped-MoO_3/MoO_3 multi-layer interconnection layer

Received 00th January 20xx,
Accepted 00th January 20xx

DOI: 10.1039/x0xx00000x

www.rsc.org/

Jian Liu[#], Shunmian Lu[#], Lu Zhu, Xinchen Li, and Wallace C. H. Choy*

In this work, we present a two-terminal perovskite (PVSK)-organic hybrid tandem solar cell with nanostructured PVSK as light window and PFN/doped MoO_3/MoO_3 structure as interconnection layer (ICL). In this tandem structure, the PVSK layer is specially designed with nanostructured surface morphology; thus the PCBM could be filled-up for forming intimately contacted interface with PVSK layers. This design could not only efficiently increase the device performance and also greatly remove the hysteresis of PVSK solar cells. The study indicates that the doped MoO_3 as the step layer plays key role in protecting the underlying layer against multi-solution processes and efficient recombination of electrons and holes generated from subcells. The hybrid tandem solar cell could achieve a high V_{OC} of 1.58 V, which is the sum of those in two sub-cells, and a high FF of 0.68, indicating the effectiveness of the multi-layer ICL.

Introduction

Photovoltaic technology has been regarded as the most promising way to produce clean energy at economic cost. Recently, organic-inorganic hybrid perovskite $(CH_3NH_3)PbX_3$ (X=Cl, Br and I) (PVSK) based solar cells have recently attracted intensive attention due to high performance, mechanical flexibility and large-area solution-processed fabrication.[1–6] So far the continuous efforts have boosted the efficiency of single-junction (SJ) PVSK solar cell over 20%,[7,8] representing the bright future for their practical application.

PVSK material is ionic polycrystalline in nature, which generates Janus effects on its application in thin film solar cells.[9,10] Firstly, ionic property endows PVSK very high dielectric constant for electrostatic force screening with the charges generated directly after light excitation.[11] On the other hand, this property makes PVSK very sensitive to external environment such as moisture and electrical bias, which brings the instability and anomalous hysteresis into the devices.[12–16] In terms of standardization of PVSK solar cells, hysteresis should be eliminated because of unstable device performance. In addition, hysteresis also hinders the development of tandem technology, which requires the photo-current matching among sub-cells.[17] Exploring the origin of the hysteresis and its solution have been considered as the critical task of future studies. Recently, Shao et al. discovered that the hysteresis might origin from the trap states of PVSK layer and interestingly surface n-type PCBM could passivate parts of them with reduced hysteresis.[18] In our recent work, the halide I^- has been identified as the dominant mobile ion in PVSK layer, which might result in hysteresis via an electrochemical process.[19] Moreover, Xu et al. directly incorporated PCBM in bulk PVSK layer and argued PCBM could stabilize I^- with reduced hysteresis.[20] Although these strategies, to some extent, resolved the hysteresis problem, there are still some concerns. For example, the PCBM layer atop of PVSK layer could merely passivate some of surface traps; while the PVSK-PCBM composite precursor requires organic solvent to stabilize PCBM molecules, which will reduce the solubility of PVSK and limit the formation of thick layer for high device efficiency. In this regards, more works should be done to develop efficient strategies for reducing the device hysteresis.

Recently, tandem solar cells using PVSK as wide band-gap absorber have attracted increasing attention due to their potential for further enhancing device efficiency.[21] C. Bailie et al. firstly demonstrated a four-terminal tandem architecture cell by integrating semi-transparent PVSK cell with transparent Ag nanowires top electrode on top of low band-gap solar cells and achieved improved device performance compared to two single-junction solar cells.[22] Similarly Philipp Lŏper et al. reported organic-inorganic halide PVSK/crystalline silicon four-terminal tandem solar cells with an efficiency of 13.4% by using transparent MoO_3/ITO top electrode.[23] In this four-terminal tandem architecture, the key factor is top transparent electrode, which currently is still a problem in terms of low cost, high transparency and large conductivity.[24] Compared to four-terminal tandem structure, two-terminal tandem architecture by connecting two sub-cells in series is much

Department of Electrical and Electronic Engineering
The University of Hong Kong, Pokfulam Road, Hong Kong, China
E-mail: chchoy@eee.hku.hk
# These authors contributed equally to his work.
†Electronic supplementary information (ESI) available. See DIO:

Nanoscale Accepted Manuscript

simple, releasing the need of top transparent electrode. The advantages of this structure have been proved in organic bulk heterojunction (BHJ) tandem community with a record efficiency of up to 12%.[25–29] However, the two-terminal tandem solar cells based on PVSK have been rarely studied. The possible reason might be the difficult of the design of interconnection layer (ICL). In two-terminal architecture, the ICL serves as charge-recombination centre and also the protection layer, dominating the final device performance. As known, PVSK layer is sensitive to aqueous /polar solvents and in addition the PVSK solar cells usually employ organic hole-transporting layer (electron-transporting layer) in regular (inverted) architecture to efficiently extract charges and reduce the recombination.[30,31] Therefore it is very difficult to build ICL and sequentially second active layer on PVSK sub-cells through solution process, considering most of near-infrared light absorbers, such as organic low-band-gap semiconductor and quantum dots, are processed by organic solvents.[32,33] Smartly, Chen et al. recently demonstrated an efficient PVSK/organic BHJ two-terminal tandem solar cell by stacking PVSK sub-cell on organic BHJ sub-cell with water/alcohol processed PFN/TiO_2/PEDOT:PSS ICL.[33] Their study indicates that organic BHJ systems are very promising as spectrally complementary absorbers in two-terminal PVSK tandem architecture and still have large space to be developed by molecular design and morphology modification. However, in this PVSK-top architecture, the incident light is firstly coming into near-infrared organic BHJ sub-cell with parts of short-wavelength photons absorbed by organic layer, which are expected to be harvested by PVSK sub-cell. The best tandem architecture should manage the photons to be converted by their specialized sub-cells in most efficient way. In this regard, the proper tandem architecture should use PVSK layer as the bottom sub-cell and organic BHJ layer as rear sub-cell. As mentioned, this tandem structure is difficult to be realized due to the multi-solution processes. For example, the PVSK layer could be destroyed by solution process of aqueous PEDOT:PSS layer even there is an organic layer such as PCBM protective layer on it. Hindered by these problems, there are still no reports on PVSK-bottom two-terminal hybrid tandem solar cells despite their importance and the insight of how to optimize the ICL in such tandem structure is still missing to date.

In this work, we presented PVSK-organic hybrid tandem solar cells with PVSK sub-cell as light window and PFN/Ag (Al)-doped MoO_3/MoO_3 as interconnection layer. In this tandem structure, the PVSK layer is specially designed with nanostructured surface morphology; thus the PCBM could be filled-up for forming intimately contacted interface with PVSK layers. This design could not only efficiently increase the device performance and also greatly remove the hysteresis of planar device. Optical modelling is implemented to guide the design of hybrid tandem solar cells and points out that the dominated factor for photocurrent in tandem cell is near-infrared organic sub-cell. The hybrid tandem solar cell could achieve a high V_{OC} of 1.58 V and a FF of 0.68, indicating the effectiveness of the multi-layer ICL. The future endeavor for performance enhancement in hybrid tandem solar cells has been also pointed out.

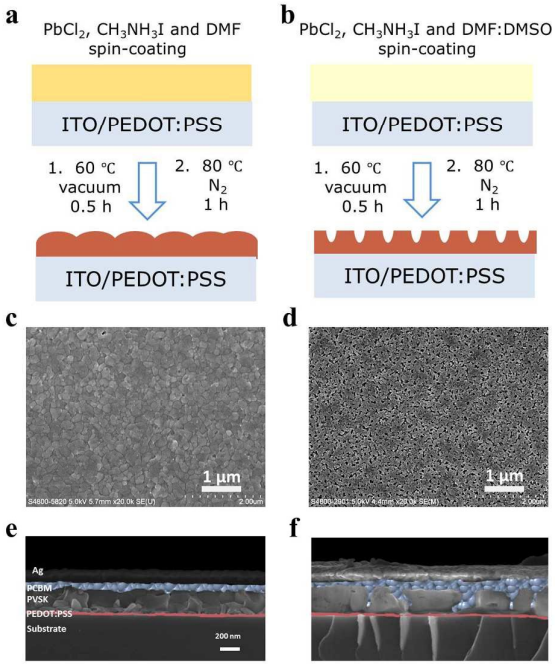

Fig. 1 The schematic formation processes of PVSK films spin-coated from DMF solution (a) and mixed solution (b); SEM images of PVSK films spin-coated from DMF solution (c) and mixed solution (d), and cross-sectional SEM of Substrate/PEDOT:PSS/PVSK layer/PCBM/Ag multilayer based on DMF-processed PVSK (e) and mixed solvent-processed PVSK layer (f).

Results and discussion

Single-junction PVSK solar cells

In this work, we use $CH_3NH_3PbI_{3-x}Cl_X$ as the PVSK absorber owing to low-temperature annealing, long charge diffusion length and smooth surface.[34,35] As for the device architecture, we choose inverted planar p-i-n structure by sandwiching PVSK layer between p-type PEDOT:PSS and n-type PCBM layer. The contact between PVSK layer and n-type PCBM is supposed to be very important to the device performance. Herein, we adopt the experience from the deposition of sol-gel film from slow-evaporating solution to shape the surface: when the speed of solvent evaporation is comparable to that of the interaction between solutes, the volume constriction due to the evaporation of solvent molecules will make the film surface shaped.[36] As schematically shown **Fig. 1**a and b, two types of PVSK layers are prepared by choosing two different recipes. The first PVSK layer is deposited by using low-boiling-

Nanoscale Accepted Manuscript

This journal is © The Royal Society of Chemistry 20xx

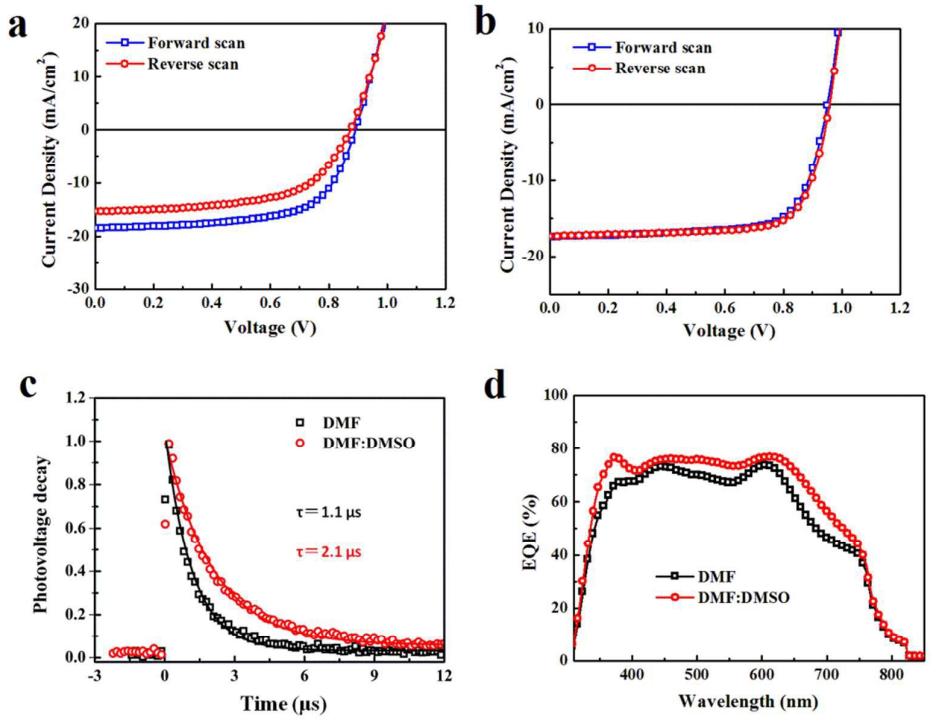

Fig. 2 The J-V characteristics of solar cells based on the boundary-featured PVSK layer(a) and nanostructured PVSK layer (b); The transient photo-voltage decay (c) and external quantum spectra (d) of PVSK solar cells.

point DMF, while the second PVSK layer uses mixed DMF:DMSO with slow-evaporating speed. Sequentially both of wet films are subjected to low-temperature thermal annealing under vacuum. For the first PVSK layer, the evaporating speed of residual DMF solvent in film is much faster than the reaction process of precursor. The obtained film is very smooth without voids. However, for the second PVSK layer, the evaporating speed of residual DMF:DMSO is comparable with that of the reaction process. Thus many voids are produced due to the volume constriction. The morphologies of two resultant PVSK films are studied by using scanning electron microscopy (SEM) and corresponding results are shown in Figure 1c and d. As seen, the PVSK layer deposited from DMF is characterized by close-packed crystals with grain size of around 200 nm and clear boundaries. On contrary, the morphology of PVSK layer from mixed solvent features uniformly distributed voids with a size of 100 nm and spacing at about 200 nm, and does not show apparent grain boundaries. It should be noted that this nanostructured PVSK film is quite different from the film with incomplete coverage reported previously, which results from the de-wetting process or the over-growth of PVSK crystals and is supposed to adversely impact device performance.[37] For the nanostructured PVSK layer, as shown in Fig. 1e and 1f, the PCBM can fill up the voids and consequently form a conformable and intimate contact with increased interfacial areas, which can contribute to improving the device performances.

Fig. 2 shows the J-V characteristics and corresponding EQE spectra of planar single-junction PVSK solar cells based on two different recipes. As shown in Fig. 2a, J-V curve of PVSK solar cells based on boundary-featured film renders severe hysteresis and corresponding parameters are listed in **Table 1**. In forward scanning direction (short circuit to positive bias), the device shows short-circuit current (J_{SC}) of 18.4 mA/cm^2, fill factor (FF) of 64.2% and overall PCE of 10.5%. In reverse direction (positive bias to short circuit), the efficiency of device was reduced to 7.97% due to the greatly reduced FF and J_{SC}. In stark contrast, the solar cells based on nanostructured PVSK film exhibit nearly the same device efficiencies (11.9% and 12.2%) in forward and reverse directions, respectively, as shown in Fig. 2b. Meanwhile the V_{OC} and FF are greatly enhanced compared to PVSK solar cells prepared from DMF solution. In previous works, it is suggested that the anomalous hysteresis of PVSK solar cells might arise from the ionic migration, charge capture/release by traps states and electrical polarization.[15] Although the real cause of hysteresis is still under debate, it is evidenced that the hysteresis could be reduced by passivating the surface traps with n-type PCBM molecules and reducing electric field-induced anion migration on boundary sites. For the PVSK film deposited from mixed

Nanoscale Accepted Manuscript

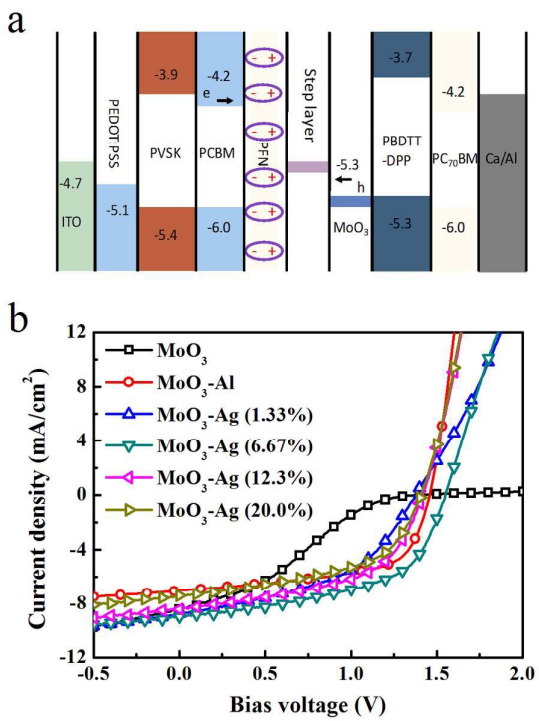

Fig. 3 (a) The device architecture with corresponding energy levels for the hybrid tandem solar cell and (b) J-V characteristics of hybrid tandem solar cells with different ICLs.

solvent, the PCBM molecules could easily filtrate into the voids, leading to increased interface area between PVSK film and n-type PCBM molecules. The enhanced interaction between two layers might enhance the passivation of surface traps and consequently reduce the hysteresis. In addition, the grain boundaries, which function as the channel of ion migration, are greatly reduced in the nanostructured film. This might also contribute to reduce the hysteresis. Transient photo-voltage decays in two types of solar cells are measured to investigate the charge dynamics along the entire pathway in Fig. 2c. The fitted lifetime of photo-generated charges are 1.1 s and 2.1 s for the solar cells prepared from DMF and mixed solution, respectively. The result indicates that the surface trap states of nanostructured PVSK could be efficiently passivated by PCBM due to the improved contact. Therefore the trap-assisted recombination channel is shut down and consequently the lifetime of photo-generated charges is prolonged. The presence of the voids in the PVSK film processed from mixed solution would, to some extent, reduce the light extinction capability, but increased photocurrent is still observed. In Fig. 2d, the external quantum efficiency (EQE) spectra are displayed. The PVSK solar cell prepared from mixed solvent shows increased photon-electron conversion efficiency with respect to the one from DMF solvent, which is consistent to the measured photocurrent.

Optimization of interconnection layer

It is very crucial to choose appropriate ICL for PVSK-organic hybrid tandem solar cells. The ICL should meet the prerequisites of protecting underlying layers from second spin-coating process and realizing the energy-loss-free charge recombination. In **Fig. 3**a, the device architecture with corresponding energy levels for the hybrid tandem solar cell is displayed. The PVSK solar cell is used as front sub-cell and organic PBDTT-DPP:$PC_{70}BM$ as rear sub-cell. The ICL employs a trip-layer structure consisting of PFN layer/step layer/MoO_3.

Table 1 Photovoltaic performance of single-junction PVSK solar cells and hybrid tandem solar cells

Single-junction PVSK solar cells					
Devices	Sweep	V_{OC} [V]	J_{SC} [mA/cm^2]	FF	PCE [%]
DMF	forward	0.89	18.4	0.642	10.5
	reverse	0.88	15.4	0.588	7.97
DMF:DMSO	forward	0.95	17.4	0.720	11.9
	reverse	0.96	17.3	0.733	12.2
Optimization of ICL					
Step layer		V_{OC} [V]	J_{SC} [mA/cm^2]	FF	PCE [%]
MoO_3		1.38	7.65	0.281	3.26
MoO_3-Al		1.45	7.02	0.611	6.17
MoO_3-Ag	1.33%	1.37	7.95	0.461	5.02
	6.67%	1.55	8.15	0.535	6.76
	13.3%	1.41	7.65	0.523	5.64
	20.0%	1.41	6.74	0.515	4.89
Optimized hybrid tandem solar cells					
Device		V_{OC} [V]	J_{SC} [mA/cm^2]	FF	PCE [%]
Hybrid tandem		1.58	8.02	0.68	8.62
Single-junction PVSK		0.88	10.3	0.73	6.61
Single-junction PBDTT-DPP:$PC_{70}BM$		0.72	14.0	0.63	6.36

Nanoscale Accepted Manuscript

This journal is © The Royal Society of Chemistry 20xx

The PFN molecules are assembled on the surface of n-type PCBM layer to form a dipole pointing from PCBM layer to step layer, which facilitates the extraction of electrons from PVSK sub-cell. The high work-function MoO_3 layer is used to form Ohmic contact with up-lying organic sub-cell for efficiently hole extraction. The key part of such trip-layer structure is the step layer serving as the recombination centre and simultaneously as the protection layer. The J-V characteristics of hybrid tandem solar cells with different step layers are demonstrated in Fig. 3b. As pristine MoO_3 film is used as step layer, J-V curve of the device shows apparent S-shaped kink with low V_{OC} of 1.38 V and low FF of 0.281. This might result from the big energy level offset between PFN and MoO_3 layers, leading to inefficient charge recombination and electrons (holes) accumulation at each side of PFN/MoO_3 interface.[38] When Al doped MoO_3 (MoO_3-Al) layer is used as step layer, the V_{OC} and FF of hybrid tandem solar cell is greatly improved up to 1.45 V and 0.611 without S-shape observed in J-V curve. The MoO_3-Al layer with medium WF of 4.5 eV could form cascade energy levels with PFN and MoO_3 layer, which facilitates the recombination of charge carriers being collected by PFN and MoO_3 layers. In addition, it is reported that the Al doping could also increase the charge carrier population and consequently conductivity of MoO_3 layer.[39] This could not only reduce the bulk resistance of oxide layer, but also decrease the width of triangle energy barrier at interface and increase the possibility of tunnelling through for charge carriers. The increased charge recombination and reduced resistance are responsible for the enhanced device performance as MoO_3-Al layer is used as step layer. To generalize this strategy, stable metallic Ag is further employed to dope MoO_3 (MoO_3-Ag) layer with varying weight ratios from 1.33% to 20.0%, which are applied as step layer in hybrid tandem solar cells. The working principle of the ICL is demonstrated in Fig. S1 (†ESI). As the Ag content increase, the WF of MoO_3-Ag layer is gradually reduced from 5.12 eV to 4.68 eV and the electrons and holes can recombine with the reduced resistance and energy losses. The optical transparency of ICL with different Ag contents is shown in Fig. S2 (†ESI). The transparency of ICLs decreases fast when the weight percentage of Ag is over 6.67%. Therefore the device exhibits the best performance with V_{OC} of 1.55 V, J_{SC} of 8.15 mA/cm^2, FF of 0.535 and overall PCE of 6.76% when the Ag content is 6.67% with the reduced WF of 4.91 eV for the step layer. The reduced J_{SC} and PCE are observed when the ratio of Ag gets high levels due to the decreased optical transparency of ICL. The metallic atoms also play a role in cross-linking oxide layer by their interaction with oxide structure and make the film robust to withstand the solvent.[40] This effect also contributes to fabricating efficient hybrid tandem solar cells with reduced energy loss in ICL.

The optical simulation

It is not a trivial work to optimize hybrid tandem solar cells as

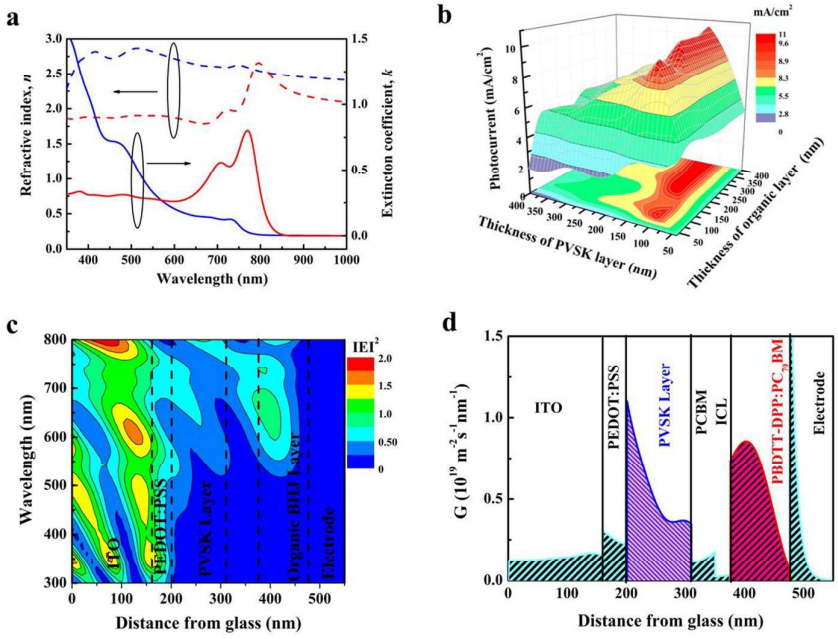

Fig. 4 (a) The optical constants (n and k) of PVSK layer (blue) and PBDTT-DPP:PC_{70}BM layer (red); (b) The 3-D mesh plot of simulated photocurrents of hybrid tandem solar cells as function of the thickness combination of PVSK layer and organic BHJ layer, and (c) Contour plot of opto-electrical field profile at different wavelengths and (d) Simulated photocurrent generation in hybrid tandem solar cell with 110-nm-thick PVSK film and 100-nm-thick organic BHJ layer.

Nanoscale Accepted Manuscript

each layer is coupled to impact the final device performance. Optical modelling has been evidenced as an effective strategy for guiding the fabrication of multilayer solar cells. **Fig. 4** shows the optical simulation in PVSK-organic hybrid tandem solar cells based on classic transfer matrix method. The optical constants of PVSK layer and PBDTT-DPP:$PC_{70}BM$ BHJ layer are measured by fitting the ellipsometry data and corresponding results are displayed in Fig. 4a. PVSK layer exhibits very strong extinction capability at short wavelength range of 300 to 600 mm while organic BHJ layer is a good absorber for the long-wavelength photons. The 3D mesh plot of simulated photo current of hybrid tandem solar cells verse the thickness combination of PVSK layer and PBDTT-DPP:$PC_{70}BM$ layer is shown in Fig. 4b. The internal quantum efficiencies (IQE) of PVSK sub-cell and organic sub-cell are assumed to be 100% and 70%, respectively. The maximum photocurrent of hybrid tandem solar cells are usually achieved when the thickness of organic sub-cell is at its interference peaks (100 nm, 200 nm and 360 nm) while the thickness of PVSK layer is limited at a range of 90 to 150 nm. The simulated result indicates that the photocurrent of hybrid tandem solar cells is dominated by that of organic sub-cells. Given the catastrophic effects of thick BHJ layer on the performance of organic sub-cells, the optimized hybrid tandem solar cells should keep the thickness of organic layer at a range of 90-120 nm and the PVSK layer at around 110 nm with an optimized photocurrent of 9.2 to 9.8 mA/cm^2. Fig. 4c shows the 2D contour plot of opto-electrical field verse the wavelength and position in hybrid tandem solar cell with 110-nm-thick PVSK layer and 100-nm-thick organic BHJ layer. As can be seen, the short wavelength photons are fully absorbed by the surface of PVSK layer and hardly penetrate into the deep place. As the wavelength of photon is increased, the photons gradually penetrate the PVSK layer and contribute to the absorption of organic sub-cell. In the range of 600-800 nm, the maximum value of opto-electrical field falls upon the middle of organic BHJ layer. In this regards, PVSK layer could function as an effective photon filter allowing the pass of long-wavelength photons and absorb the short-wavelength photons, which could improve the utilization efficiency of light and finally boost the device performance.[41] Fig. 4d shows the spatial distribution profile of photo-generated chargers in hybrid tandem solar cells. The generation of charges in PVSK sub-cell mainly happens at the surface part due to the contribution of short wavelength light extinction while the long wavelength photons are converted into charges at the middle of BHJ layer. Although the electrons in PVSK sub-cell are required to drift a longer distance than holes generated in organic sub-cell to reach ICL for combination, the balanced recombination is expected as the charge mobility of PVSK layer is much higher than that of organic BHJ layer. This is very distinct from the case in polymer tandem solar cells, where the unbalanced recombination is supposed to adversely impact the device performance with reduced FF.[40] In this regard, PVSK-organic hybrid tandem solar cells might be a promising way of converting large-range light into electricity.

PVSK-organic hybrid tandem solar cells

According to the guideline of the optical modelling, the optimized hybrid tandem solar cells are fabricated with the thicknesses of PVSK layer and PBDTT-DPP:$PC_{70}BM$ layer at around 110 nm and 100-120 nm, respectively. The ICL employs PFN/MoO_3-Ag (6.67%, 15 nm)/MoO_3 (10nm) multi-layer architecture. The J-V characteristics of hybrid tandem solar cell and corresponding single-junction reference cells are displayed in **Fig. 5**a and corresponding results are listed in Table 1. The best hybrid tandem solar cell achieves a V_{OC} of 1.58 V, a J_{SC} of 8.02 mA/cm^2, a FF of 0.68 and overall PCE of 8.62%, which is higher than those (6.61% and 6.36%) in two sub-cells. The V_{OC} of hybrid tandem device is the sum of those (0.88 V and 0.72 V) in two sub-cells, indicating the electrons generated in PVSK sub-cell could efficiently recombine with the holes from the

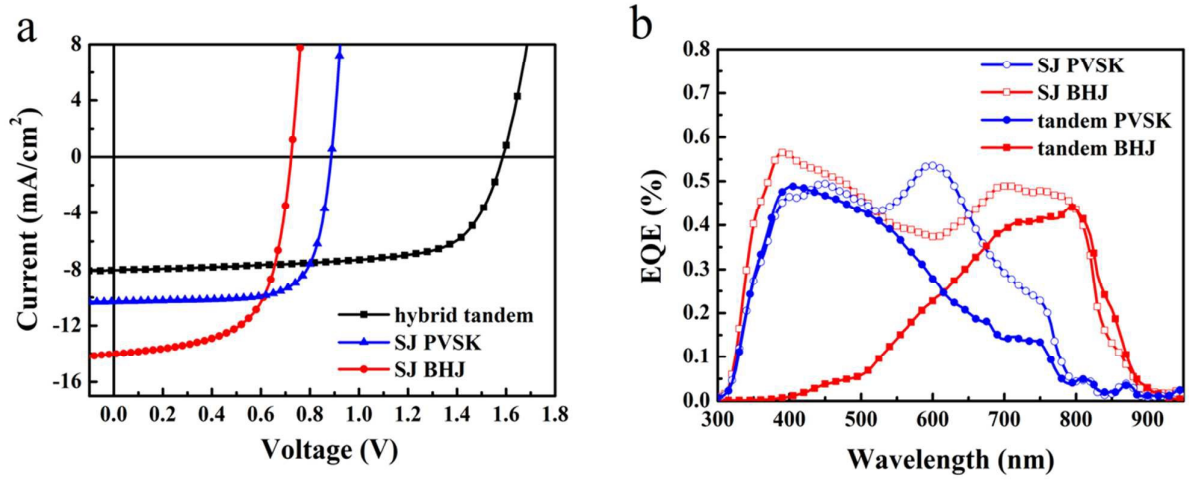

Fig. 5 (a) J-V characteristics of single-junction PVSK and PBDTT-DPP:$PC_{70}BM$ reference solar cells and hybrid tandem solar cell; (b) EQE spectra of two sub-cells in hybrid tandem solar cells and corresponding single-junction reference solar cells.

Nanoscale Accepted Manuscript

This journal is © The Royal Society of Chemistry 20xx

organic sub-cell with ignorable energy loss. The relatively high FF value implies the small resistance of ICL and the absence of the charges accumulation at ICL due to the efficient charge recombination. External quantum efficiency (EQE) spectra of corresponding solar cells are demonstrated in Fig. 5b. The PVSK and organic BHJ sub-cells, which convert short-wavelength and long-wavelength light, respectively, achieve matched photocurrent. It is noted that the J_{SC} of hybrid tandem solar cell is only 8.02 mA/cm^2, which is lower than the predicted value of 9.3 mA/cm^2 in the optical modelling part. The discrepancy mainly results from the less efficient organic sub-cell than the assumed value in optical modelling. The photocurrent of hybrid tandem solar cell is dominated by that generated in organic infrared sub-cell. It is envisioned that the advanced design of organic infrared materials by increasing the mobility for efficient photon-electron conversion and reducing the spectral overlap with PVSK could push the device performance of such hybrid tandem solar cells up to an encouraging level.

Conclusions

In this work, we report PVSK-organic hybrid tandem solar cell based on nanostructured PVSK layer as light window and PFN/doped-MoO_3/MoO_3 multi-layer ICL. Nano-structured engineering of PVSK layer has been proved to be an effective strategy for enhancing the electronic coupling between PVSK layer and n-type PCBM, which helps to reduce the trap states and eliminate the device hysteresis. The optical modelling is used to guide the fabrication of such hybrid tandem solar cells. The simulation result indicates that the PVSK layer could function as an effective filter for converting short-wavelength photons and allowing the pass of long-wavelength photons to be used in near-infrared sub-cell. The best hybrid tandem solar cell achieves V_{OC} of 1.58 V, which is the sum of those in two sub-cells, and a high FF of 0.68. This indicates the effectiveness of ICL, allowing the charges to recombine without energy loss. It is expected that the development of advanced organic infrared photo-active materials will push the efficiency of such hybrid tandem solar cells up to a higher level.

Experimental section

Materials

PBDTT-DPP polymer & PFN, PCBM and $PC_{70}BM$ were purchased from 1-Material Inc, Solarmer Materials Inc. and Nano-C, respectively. CH_3NH_3I was synthesized by following the reported procedure.[4] The $PbCl_2$ (Aldrich) and CH_3NH_3I were mixed in DMF or mixed DMF/DMSO (0.8:0.2 in Volume) at molar ratio of 1:3 with different weight percentages.

Single-junction device fabrication

ITO coated glass slides were cleaned by ultra-sonication for 30 minutes in detergent water, de-ionized water, acetone and ethanol sequentially. The ITO substrates were then subjected to UVO treatment for 25 minutes. The PEDOT:PSS layer were spin-coated on ITO substrates. For the single-junction planar PVSK solar cells, the precursor in mixed DMF/DMSO solvent (60 wt %) was spin-coated on PEDOT:PSS layer. As reference, the precursor in DMF solvent (60 wt %) was also spin-coated on PEDOT:PSS layer. The obtained films were subjected to low-temperature (60℃) annealing under vacuum condition for 40 minutes in order to remove the solvent. Then the sequential films were annealed at 80℃ for one hour to transfer into PVSK layers with thickness of 220 nm. Then 40-nm-thick PCBM layer was deposited on PVSK layer as n-type layer and PFN film with a thickness of 1 nm was spin-coated as interfacial layer. Finally the 80-nm-thick Ag was thermally deposited as the cathode. For single-junction organic solar cells, the PBDTT-DPP/$PC_{70}BM$ blended solution (1:2,18 mg/ml in 1,2-dichlorobenzene o-DCB) was spin-coated on PEDOT:PSS layer to form 110-nm-thick layer.Ca (20 nm)/Al (100 nm) were sequentially thermal-evaporated as the cathode. The area of the cells was 0.06 cm^2 defined by the mask.

Tandem device fabrication

The fabrication of the front sub-cell mainly followed the procedure for the preparation of the single-junction device until the Ag cathode was deposited. The only difference was the variation of the PVSK layer thickness for the optimization of tandem devices. Sequentially, the Ag or Al doped MoO_3/MoO_3 bi-layer was deposited as interconnection layer, where the co-evaporation technique was used for doped MoO_3 layer deposition. The content of Al in MoO_3-Al step layer keeps between 40% and 50% wt %. The PBDTT-DPP/$PC_{70}BM$ blended solution (1:2, 18 mg/ml in 1,2-dichlorobenzene o-DCB) was spin-coated on PEDOT:PSS layer to form 110-nm-thick layer. Ca (20 nm)/Al (100 nm) were sequentially thermal-evaporated as the cathode. The area of the cells was 0.06 cm^2 defined by the mask.

Device characterization

The work functions of different layers were measured by Kelvin probe. The morphology of PVSK layers on ITO/PEDOT:PSS substrates were characterized by scanning electron microscopy (SEM, Hitachi S-4800).The refractive index (*n* and *k* values) of the layers in the device structure was measured using a VASE ellipsometer from J. A.Woollam Co., Inc. Current density-voltage (*J-V*) characteristics were obtained by using a Keithley 2635 source meter and Newport AM 1.5G solar simulator with irradiation intensity of 100 mW cm^{-2}. The thicknesses of layers were measured by a Dekak Stylus Profiler.

Acknowledgements

This work was supported by the University Grant Council of the University of Hong Kong (Grant 104003463), the general Research Fund (Grants HKU711813 And HKU711612E), an RGC-NSFC Grant (N HKU709/12), the collaborative Research Fund (grant CUHK1/CRF/12G) from the Research Grants Council of Hong Kong Special Administrative Region, China, and Grant CAS14601 from CAS-Croucher Funding Scheme for Joint Laboratories. We thank Hong Zhang for the technical support in material synthesis.

Nanoscale Accepted Manuscript

References

1 M. Grätzel, *Nat. Mater.*, 2014, **13**, 838–842.

2 S. Kazim, M. K. Nazeeruddin, M. Grätzel and S. Ahmad, *Angew. Chem. Int. Ed. Engl.*, 2014, **53**, 2812–24.

3 O. Malinkiewicz, A. Yella, Y. H. Lee, G. M. Espallargas, M. Graetzel, M. K. Nazeeruddin and H. J. Bolink, *Nat. Photonics*, 2013, **8**, 128–132.

4 H. Zhang, J. Mao, H. He, D. Zhang, H. L. Zhu, F. Xie, K. S. Wong, M. Grätzel and W. C. H. Choy, *Adv. Energy Mater.*, 2015, n/a–n/a.

5 J. M. Ball, M. M. Lee, A. Hey and H. J. Snaith, *Energy Environ. Sci.*, 2013, **6**, 1739.

6 W. E. I. Sha, X. Ren, L. Chen and W. C. H. Choy, *Appl. Phys. Lett.*, 2015, **106**, 221104.

7 W. S. Yang, J. H. Noh, N. J. Jeon, Y. C. Kim, S. Ryu, J. Seo and S. I. Seok, *Science (80-.).*, 2015, **348**, 1234–7.

8 H. Zhou, Q. Chen, G. Li, S. Luo, T. -b. Song, H.-S. Duan, Z. Hong, J. You, Y. Liu and Y. Yang, *Science (80-.).*, 2014, **345**, 542–546.

9 C. Eames, J. M. Frost, P. R. F. Barnes, B. C. O'Regan, A. Walsh and M. S. Islam, *Nat. Commun.*, 2015, **6**, 7497.

10 J. Haruyama, K. Sodeyama, L. Han and Y. Tateyama, *J. Am. Chem. Soc.*, 2015, **137**, 150810155937002.

11 Q. Lin, A. Armin, R. C. R. Nagiri, P. L. Burn and P. Meredith, *Nat. Photonics*, 2014, **9**, 106–112.

12 T. Leijtens, G. E. Eperon, N. K. Noel, S. N. Habisreutinger, A. Petrozza and H. J. Snaith, *Adv. Energy Mater.*, 2015, n/a–n/a.

13 B. Wu, K. Fu, N. Yantara, G. Xing, S. Sun, T. C. Sum and N. Mathews, *Adv. Energy Mater.*, 2015, **5**, n/a–n/a.

14 E. L. Unger, E. T. Hoke, C. D. Bailie, W. H. Nguyen, A. R. Bowring, T. Heumuller, M. G. Christoforo and M. D. McGehee, *Energy Environ. Sci.*, 2014, **7**, 3690–3698.

15 H. J. Snaith, A. Abate, J. M. Ball, G. E. Eperon, T. Leijtens, N. K. Noel, S. D. Stranks, J. T.-W. Wang, K. Wojciechowski and W. Zhang, *J. Phys. Chem. Lett.*, 2014, **5**, 1511–1515.

16 M. D. McGehee, *Nat. Mater.*, 2014, **13**, 845–846.

17 T. Ameri, N. Li and C. J. Brabec, *Energy Environ. Sci.*, 2013, **6**, 2390.

18 Y. Shao, Z. Xiao, C. Bi, Y. Yuan and J. Huang, *Nat. Commun.*, 2014, **5**, 5784.

19 H. Zhang, H. Lin, C. Liang, H. Liu, J. Liang, Y. Zhao, W. Zhang, M. Sun, W. Xiao, H. Li, S. Polizzi, D. Li, F. Zhang, Z. He and W. C. H. Choy, *Adv. Funct. Mater.*, 2015, in pess.

20 J. Xu, A. Buin, A. H. Ip, W. Li, O. Voznyy, R. Comin, M. Yuan, S. Jeon, Z. Ning, J. J. McDowell, P. Kanjanaboos, J.-P. Sun, X. Lan, L. N. Quan, D. H. Kim, I. G. Hill, P. Maksymovych and E. H. Sargent, *Nat. Commun.*, 2015, **6**, 7081.

21 F. Lang, M. A. Gluba, S. Albrecht, J. Rappich, L. Korte, B. Rech and N. H. Nickel, *J. Phys. Chem. Lett.*, 2015, **6**, 2745–50.

22 C. D. Bailie, M. G. Christoforo, J. P. Mailoa, A. R. Bowring, E. L. Unger, W. H. Nguyen, J. burschka, N. Pellet, J. Z. Lee, M. Grätzel, R. Noufi, T. Buonassisi, A. Salleo and M. D. McGehee, *Energy Environ. Sci.*, 2014, **8**, 956–963.

23 P. Löper, S.-J. Moon, S. M. de Nicolas, B. Niesen, M. Ledinsky, S. Nicolay, J. Bailat, J.-H. Yum, S. De Wolf and C. Ballif, *Phys. Chem. Chem. Phys.*, 2015, **17**, 1619–29.

24 D. S. Hecht, L. Hu and G. Irvin, *Adv. Mater.*, 2011, **23**, 1482–513.

25 J. You, L. Dou, Z. Hong, G. Li and Y. Yang, *Prog. Polym. Sci.*, 2013, **38**, 1909–1928.

26. Press release: http://www.heliatek.com/newscenter/latest_news/neuer-weltrekord-fur-organische-salarzellen-heliatek-behaupter-sjch-mit-12-zellettizienz-als-technologiefuhrer/?lang=en.

27 C.-C. Chen, W.-H. Chang, K. Yoshimura, K. Ohya, J. You, J. Gao, Z. Hong and Y. Yang, *Adv. Mater.*, 2014, **26**, 5670–7.

28 J. You, C.-C. Chen, Z. Hong, K. Yoshimura, K. Ohya, R. Xu, S. Ye, J. Gao, G. Li and Y. Yang, *Adv. Mater.*, 2013, **25**, 3973–3978.

29 S. Lu, X. Guan, X. Li, W. E. I. Sha, F. Xie, H. Liu, J. Wang, F. Huang and W. C. H. Choy, *Adv. Energy Mater.*, 2015, **5**, n/a–n/a.

30 M. M. Lee, J. Teuscher, T. Miyasaka, T. N. Murakami and H. J. Snaith, *Science*, 2012, **338**, 643–7.

31 J. Seo, S. Park, Y. Chan Kim, N. J. Jeon, J. H. Noh, S. C. Yoon and S. Il Seok, *Energy Environ. Sci.*, 2014, **7**, 2642.

32 S. Shao, K. Zheng, T. Pullerits and F. Zhang, *ACS Appl. Mater. Interfaces*, 2013, **5**, 380–5.

Nanoscale Accepted Manuscript

This journal is © The Royal Society of Chemistry 20xx

Please do not adjust margins

33 C.-C. Chen, S.-H. Bae, W.-H. Chang, Z. Hong, G. Li, Q. Chen, H. Zhou and Y. Yang, *Mater. Horiz.*, 2015, **2**, 203–211.

34 P. Docampo, J. M. Ball, M. Darwich, G. E. Eperon and H. J. Snaith, *Nat. Commun.*, 2013, **4**, 2761.

35 F. X. Xie, D. Zhang, H. Su, X. Ren, K. S. Wong, M. Grätzel and W. C. H. Choy, *ACS Nano*, 2015, **9**, 639–46.

36 J. Liu, S. Shao, B. Meng, G. Fang, Z. Xie, L. Wang and X. Li, *Appl. Phys. Lett.*, 2012, **100**, 213906.

37 G. E. Eperon, V. M. Burlakov, P. Docampo, A. Goriely and H. J. Snaith, *Adv. Funct. Mater.*, 2014, **24**, 151–157.

38 J. C. Wang, X. C. Ren, S. Q. Shi, C. W. Leung and P. K. L. Chan, *Org. Electron.*, 2011, **12**, 880–885.

39 J. Liu, S. Shao, G. Fang, B. Meng, Z. Xie and L. Wang, *Adv. Mater.*, 2012, **24**, 2774–9.

40 J. Liu, S. Shao, G. Fang, J. Wang, B. Meng, Z. Xie and L. Wang, *Sol. Energy Mater. Sol. Cells*, 2014, **120**, 744–750.

41 K. Xiong, S. Lu, J. Dong, T. Zhou, D. Jiang, R. Wang and H. Yang, *Sol. Energy*, 2010, **84**, 1975–1978.

TOC

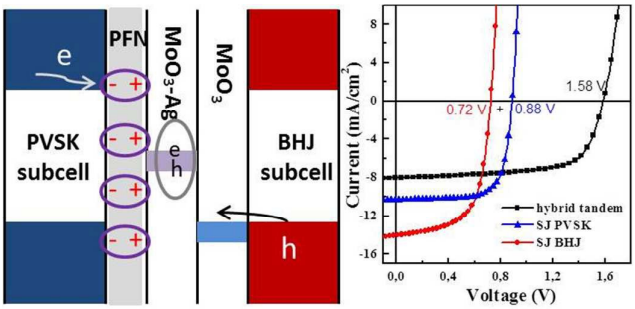

A two-terminal Perovskite (PVSK)-organic hybrid tandem solar cell with nanostructured PVSK layer as light window and PFN/doped MoO_3/MoO_3 multilayer interconnection layer is presented.

Nanoscale Accepted Manuscript